Article

Tube-like Gold Clusters $M_2@Au_{17}^q$ (M = W, Mo; q = 0, $\pm$1): Structure, Electronic Property, and Optical Nonlinearity

Pham Vu Nhat, Nguyen Thi Bao Trang, Minh Triet Dang, Nguyen Thanh Si, Tran Thi Ngoc Thao, Pham Thi Bich Thao, and Minh Tho Nguyen*

Read Online

ACCESS | Metrics & More | Article Recommendations | Supporting Information

ABSTRACT: Density functional theory (DFT) calculations are carried out to determine the geometries and electronic and nonlinear optical (NLO) properties of the doubly doped gold clusters in three charge states $M_2 @ Au_{17}^q$ with M = W, Mo and q = 0, $\pm$1. At their lowest-lying equilibrium structures, the impurities that are vertically encapsulated inside a cylindrical gold framework, significantly enhance the stability and modify properties of the host. The presence of M_2 units results in the formation of a tube-like ground state, which is identified for the first time for gold clusters. Having 30 itinerant electrons, the electron shell of $M_2@Au_{17}$ can be described as $1S^2 1P^6 1D^{10} 2S^2 \{1F_{xz}^2 1F_{yz}^2\} 1F_{z^3}^2 \{1F_{xyz}^2 1F_{z(x^2-y^2)}^2\} \{1F_{y(3x^2-y^2)}, 1F_{x(x^2-3y^2)}\}$. The species is thus stabilized upon doping, but it is not a magic cluster. The optical transitions are shifted to the lower-energy region upon doping Mo and W atoms into Au_{17}^q. The static and dynamic NLO properties of $M_2@Au_{17}^q$ are also computed and compared to those of the pure Au_{19}^q (having the same number of atoms) and an external reference molecule, i.e., para-nitroaniline (p-NA). For hyperpolarizabilities, the doped clusters possess smaller values than those of their pure counterparts but much larger values than the p-NA. Of the doubly doped systems, the neutral $M_2@Au_{17}$ exhibits particularly high first and second hyperpolarizability tensors. The doped cluster units can also be used as building blocks for the design of gold-based nanowires with outstanding electronic and optical characteristics.
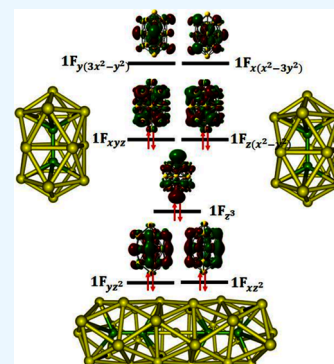
1. INTRODUCTION

There has been continuously growing attention in metal clusters as a deep understanding of their structure and physicochemical properties provides us with a bridge between their isolated atoms or molecules and their bulk materials. In particular, numerous experimental and theoretical studies have been devoted to gold clusters in recent times to emphasize their nonconventional properties due to the relativistic effects, and in part due to important applications in the fields of catalysis,[1−3] chemical/biological sensors,[4] and biomedical sciences.[5] Contrary to the peculiar inertness of its bulk, gold in the nanoscale form or when finely dispersed on metal oxide surfaces typically exerts an efficient catalytic activity for many gas-phase reactions.[6,7] In addition, gold nanomaterials are willing to conjugate to a variety of bimolecular systems and induce a much lower toxicity to human bodies than many other metallic elements.[8] Therefore, gold nanoparticles are more and more frequently employed in medical applications such as drug delivery systems.[9,10] Moreover, they possess superior optical properties as compared to other transition metals, and thus have attracted a great deal of interest in the field of biosensors and biomedical diagnostics.[11−13] It can be argued that gold nanoclusters are among the most characterized atomic aggregates to date by both experimental techniques,[14−17] and computational methods.[18−22]

Investigations into doping with foreign metals in pure gold clusters have also arisen in recent times. The presence of a doping element is expected to effectively improve the pure host properties in a more desirable fashion. A combined experimental and theoretical study using trapped ion electron diffraction, photoelectron spectroscopy, and density functional theory (DFT) confirmed the existence of highly symmetric golden cages $M@Au_{16}^-$ (M = Fe, Co, Ni, Cu).[23] It was noticeably found that although the magnetic moment of the impurity is slightly reduced, the host framework could play as a suitable accommodation to protect the magnetism of the dopant atom.[24,25] Other golden cages, i.e., $M@Au_{12}$ and $M@Au_{17}$, with M being a transition metal, were also found to possess a high thermodynamic stability and significantly improved frontier orbital energy gaps.[26−28] The effects of dopant atoms on the spectroscopic properties and reactivity of small gold clusters toward nucleophilic reagents have also been extensively reported.[29−32] Besides singly doped systems, multiply metal-doped gold clusters have also attracted an
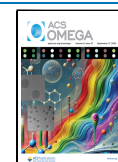
increasing interest for their unexpected properties and promising applications.[33−35] Recent DFT calculations combined with photoelectron spectroscopy[36,37] have observed high symmetry structures and particularly thermodynamic stability of bimetallic gold clusters doped with the Nb_2 unit. Such an observation is expected to open an avenue for making a new class of mixed clusters having tailor-made properties.

There is also a continuing interest in materials with pronounced nonlinear optical (NLO) responses since they were used for various optoelectronic applications including optical computing, data storage, image processing, optical switches for photonics, optical fibers, and optical signal processing.[38,39] It has been well established in the recent literature that gold-containing nanoscale materials typically exhibit excellent NLO properties.[40] Moreover, doping with other transition metals is also expected to significantly improve the NLO response of gold-based clusters.[41] While linear and NLO properties of pure gold and singly doped clusters with another metal element have been reported,[40,42] such information for the doubly doped gold clusters remains rather limited.

In this context, we report in the present paper some remarkable effects induced by the dimeric Mo_2 and W_2 units not only on the geometry and stability but also on the NLO response of gold clusters. Even though small, pure Au_n clusters with $n < 10$ tend to exist as planar or quasi-planar shapes, while larger sizes up to $n = 18$ tend to exist as hollow cages,[20,22,43] we report here, for the first time, that a triple-ring cylindrical form turns out to be the most preferred structure of the doubly doped $M_2@Au_{17}^q$ clusters with the dopant M = W, Mo in the charge states $q = 0, \pm1$. At the equilibrium points, the tube-like geometry of the Au_{17} size, which is not an equilibrium structure, is significantly stabilized by the M_2 dimers vertically placed inside the golden spindle-like framework. We in addition examine the electronic structures and effects of such dopant metals on the polarizability and first and second hyperpolarizability parameters that usually characterize the NLO properties. Our computed results show that doping with an M_2 dimer containing a strong bond such as Mo_2 or W_2 can be an effective approach to enhance the stability in a tubular form and tune the NLO properties of the resulting gold nanomaterials.

2. COMPUTATIONAL METHODS

Geometry optimizations of the $M_2@Au_{17}^{0/\pm1}$ clusters are carried out through DFT calculations using the exchange-correlation functional TPSS,[44] in conjunction with a scalar relativistic effective core potential (ECP) basis set, namely the cc-pVDZ-PP.[45] Such a basis is widely used to model heavy metal atoms as it can significantly reduce the computational cost while still yielding reliable results for many properties of systems considered.[18,45] The TPSS functional has been found to be successful in predicting the equilibrium geometry of small gold clusters.[20,22] Initial geometries of doped clusters are extensively generated using both the genetic algorithm and an empirical search using the previously known structures of the sizes Au_{17}, Au_{18}, and Au_{19} as starting points. Harmonic vibrational frequencies are subsequently calculated for optimized structures to determine their nature on the potential energy surface and to generate their zero-point energies and thermal correction values. All calculations in this study are performed using the Gaussian 16 program.[46]

In order to examine the LO and NLO responses of studied clusters, we compute the permanent dipole moment (μ), along with polarizability (α), and first and second hyperpolarizability (β and γ) in their ground state structures. Mathematically, the μ, α, β, and γ parameters are computed by eqs 1−8.[19]

$$\alpha_{iso} = \frac{1}{3}(\alpha_{xx} + \alpha_{yy} + \alpha_{zz}) \tag{1}$$

$$\alpha_{aniso} = \left[\frac{\left(\alpha_{xx} - \alpha_{yy}\right)^2 + \left(\alpha_{xx} - \alpha_{zz}\right)^2 + \left(\alpha_{yy} - \alpha_{zz}\right)^2 + 6\left(\alpha_{xy}^2 + \alpha_{xz}^2 + \alpha_{yz}^2\right)}{2} \right]^{\frac{1}{2}} \tag{2}$$

$$\beta_{tot} = [\beta_x^2 + \beta_y^2 + \beta_z^2]^{1/2} \tag{3}$$

$$\beta_i = \frac{1}{3}\sum_j (\beta_{ijj} + \beta_{jji} + \beta_{jij}), \quad i, j = \{x, y, z\}$$

$$\beta_{\parallel} = \frac{3}{5}\sum_i \frac{\mu_i \beta_i}{|\mu_i|} \tag{4}$$

$$\beta_{\perp(z)} = \frac{1}{5}\sum_j (2\beta_{zjj} - 3\beta_{jzj} + 2\beta_{jjz}) \tag{5}$$

$$\gamma_{tot} = (\gamma_x^2 + \gamma_y^2 + \gamma_y^2)^{1/2} \tag{6}$$

$$\gamma_{\parallel} = \gamma_x + \gamma_y + \gamma_z \tag{7}$$

$$\gamma_i = \frac{1}{15}\sum_j (\gamma_{ijji} + \gamma_{ijij} + \gamma_{iijj}), \quad i, j = \{x, y, z\}$$

$$\gamma_{\perp} = \frac{1}{15}\sum_i\sum_j (2\gamma_{ijji} - \gamma_{iijj}), \quad i, j = \{x, y, z\} \tag{8}$$

where α_{ij}, β_{ijk}, and γ_{ijkl} are the tensor components of polarizability, first hyperpolarizability, and second hyperpolarizability, respectively. The origin of the permanent dipole moment computed by default is the center of mass if the chemical system is neutral; otherwise, the center of nuclear charge is used as the origin.

The energy difference between the highest occupied molecular orbital (HOMO) and the lowest unoccupied molecular orbital (LUMO), i.e., HOMO−LUMO energy gap (HLG), is computed by the following equation:

$$\text{HLG} = \text{vIE} - \text{vEA} \tag{9}$$

This is a plausible approach, as according to the Koopmans theorem, HOMO and LUMO energies are directly related to the vertical ionization energy (vIE) and vertical electron affinity (vEA) values, respectively.[47] If there is no geometry relaxation during the ionization process, the energy difference between a cation and its neutral counterpart can be approached by the HOMO energy of the latter. Similarly, by applying the Koopmans theorem, one can derive a relation of the LUMO energy to the vEA value. We can also compute the HLG values by taking the HOMO and LUMO energies from the DFT computations. However, it should be noted that the electronic structure of transition metal clusters is typically multiconfigurational due to the existence of several quasi-degenerate electronic states.[48] Therefore, most of the current

DFT approaches normally yield large error margins, up to dozens of kcal/mol, for energies of both HOMO and LUMO levels because they are derived from unbalanced treatment of electron correlation.[49,50]

3. RESULTS AND DISCUSSION

3.1. Equilibrium Structures. Local minima detected for the anions $M_2@Au_{17}^-$ (M = Mo, W) at the TPSS/cc-pVDZ-PP level are displayed in Figure 1, while their Cartesian
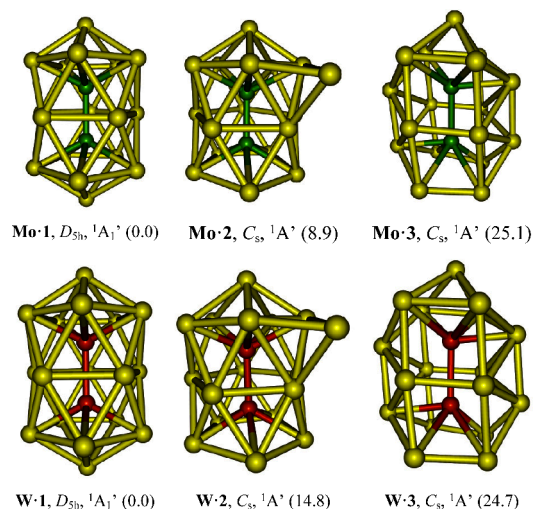

Figure 1. Some low-lying isomers of $M_2@Au_{17}^-$ (M = W, Mo) clusters along with the symmetry point group and relative energy with respect to the most stable form **M·1**. Relative energies given kcal/mol in parentheses are obtained from TPSS/cc-pVDZ-PP + ZPE computations.

coordinates are given in Table S1 of Supporting Information. At the equilibrium point, the lowest-lying clusters tend to exist as spindle-like structures, i.e., **Mo·1** and **W·1** in Figure 1, composing of three five-membered Au rings Au_{15} encapsulated with the M_2 unit inside along the axis. The next stable isomer **Mo·2** located for $Mo_2@Au_{17}^-$ is computed to be ~15 kcal/mol higher in energy. The remaining structure **Mo·3** is even much less stable as it is lying about 25 kcal/mol above **Mo·1**. Comparable structural arrangements are also obtained for $Au_{17}W_2^q$ species. While the energy difference between **W·1** and **W·2** conformations is around 15 kcal/mol, the third isomer **W·3** is predicted to be less stable than **W·1** by 25 kcal/mol. Overall, these results indicate that for the first time a gold cluster is obviously found to be favored in the tube-like form **M·1**. Numerous studies have been devoted to gold clusters functionalized with organic ligands, and the formation of either

cylindrical or anisotropic structures has been found for several ligand-protected gold clusters such as $Au_{22}(dppo)_6$,[51] and $M_2Au_{36}(SR)_{24}$ (M = Au, Pd, Pt).[52] However, the detection of such a structural motif with the dimer M_2 encapsulated inside the Au_{17} tubular shell is of importance, as this is the first discovery in gas-phase gold clusters of such a form, which is rather popular in other classes of atomic clusters.

Removal of one electron from the anions $M_2@Au_{17}^-$ to form the neutral $M_2@Au_{15}$ is accompanied by a minor structural modification. Both neutral $Mo_2@Au_{17}$ and $W_2@Au_{17}$ clusters still adopt a tubular motif similar to that of **M·1** as their global minima. However, owing to an open-shell electronic structure, they tend to undergo a Jahn–Teller distortion, giving rise to a lower symmetry structure, instead of a regular pentagonal D_{5h} spindle-like structure as in the corresponding anions. Indeed, the ground state structure of $M_2@Au_{17}$ now has a symmetry of C_s and a doublet $^2A''$ electronic state. The second most stable isomers **M·2** are computed to be less stable than **M·1** by ~9 and ~12 kcal/mol for $Mo_2@Au_{17}^-$ and $W_2@Au_{17}^-$, respectively.

Similarly, the cations $M_2@Au_{17}^+$ also prefer to exist as a lower symmetry configuration (C_{2v}), which are derived from a slightly structural relaxation of the regular pentagonal D_{5h} spindle. However, while $W_2@Au_{17}^+$ prefers a low spin electronic ground state ($^1A_1$), the triplet $^3B_1$ state is predicted to be the lowest-lying energy for $Mo_2 @ Au_{17}^+$. The singlet $^1A_1$ state of **Mo·1** is the first excited state for $Mo_2@Au_{17}^+$ with a minor energy gap of ~1 kcal/mol above the $^3B_1$ state (TPSS value). Such a tiny energy gap suggests a quasi-degeneracy of these two electronic states. The remaining isomers **M·2** and **M·3** (Figure 1) are also located as local minima on the potential energy surface of both $Mo_2@Au_{17}^+$ and $W_2@Au_{17}^+$. Their symmetry, electronic states, and relative energies corresponding to the most stable form **M·1** are given in Table 1.

The M−M bond lengths in the **M·1** equilibrium structures are computed to be 2.54 and 2.65 Å for $Mo_2@Au_{17}^-$ and $W_2@Au_{17}^-$, respectively, that are longer than the corresponding M−M distances of 1.94 and 2.02 Å in isolated Mo_2 and W_2 dimers. Our computed bond length of 1.941 Å obtained for Mo_2 is comparable to the corresponding experimental value of 1.938 Å,[21] while that of 2.017 Å of W_2 is also quite close to the previous CCSD(T) value of 2.020 Å.[53] The Mo−Mo bond distances in $Mo_2@Au_{17}$ and $Mo_2@Au_{17}^+$ are computed to be about 2.50 and 2.47 Å, respectively, which are slightly shorter than the value of 2.54 Å in $Mo_2@Au_{17}^-$. Similarly, the W−W bond length of 2.58 Å in the cation $W_2@Au_{17}^+$ is also shorter than the corresponding values of 2.61 and 2.65 Å in $W_2@Au_{17}$ and $W_2@Au_{17}^-$, respectively. Overall, the M−M distances are decreased in the order $M_2@Au_{17}^- > M_2@Au_{17} > M_2@Au_{17}^+$. In other words, electron detachment tends to strengthen the M−M bonding interaction.

Table 1. Symmetry Point Group, Electronic State, and Relative Energy (RE, kcal/mol) of Low-Lying States Obtained for $Au_{17}M_2^{0/\pm1}$ Clusters at the TPSS/cc-pVDZ-PP + ZPE Level

	$M_2@Au_{17}^-$			$M_2@Au_{17}$			$M_2@Au_{17}^+$		
isomer	symmetry	state	RE	symmetry	state	RE	symmetry	state	RE
Mo·1	D_{5h}	$^1A_1'$	0.0	C_s	$^2A''$	0.0	C_{2v}	$^3B_1$	0.0
Mo·2	C_s	$^1A'$	14.5	C_s	$^2A'$	8.9	C_s	$^1A'$	3.6
Mo·3	C_s	$^1A'$	25.1	C_s	$^2A'$	21.1	C_s	$^1A_1$	12.7
W·1	D_{5h}	$^1A_1'$	0.0	C_s	$^2A''$	0.0	C_{2v}	$^1A_1$	0.0
W·2	C_s	$^1A'$	14.8	C_s	$^2A'$	12.0	C_s	$^1A'$	4.4
W·3	C_s	$^1A'$	24.7	C_s	$^2A'$	20.6	C_1	^1A	10.4

Recent quantum chemical calculations combined with far-IR multiple photon dissociation (FIR-MPD) spectroscopy confirmed that the neutral Au_{17} favors a star-like form,[22] whereas a hollow cage[54] and an amorphous form[55] are located for Au_{17}^- and Au_{17}^+, respectively. On the contrary, while the cation Au_{19}^+ tends to exist as a hollow cage (cf. Figure S1 of Supporting Information), its neutral and anionic states are likely to exist as a truncated pyramid.[56] It is clearly seen for small gold clusters up to Au_{20} that the cylinder-like shape is not even a local minimum on the energy potential surface, and removing or adding an electron typically leads to a substantial tune on their structures. With the presence of dimer M_2, the cylindrical conformation turns out to be the most preferred structure of $M_2@Au_{17}^q$ species. Moreover, unlike the pure systems, the doped counterparts undergo a minor structural modification upon electron removal or addition.

3.2. Effects of Dopants on the Stability of Gold Clusters.

The stability of clusters is usually evaluated via the binding energy per atom (BE) and the detachment energy (DE). As shown in Table 2, both Au^- and Au are much more

Table 2. Electron Affinity (EA) and Ionization Energy (IE) of Elements, Clusters, and Dimers in Gas Phase[a]

	Au	W	Mo	Au_{17}	W_2	Mo_2
EA (eV)	2.31	0.82	0.75	3.72	0.90	0.67
IE (eV)	9.22	7.98	7.09	6.55	6.61	7.53

[a]Experimental values for Au, W, and Mo are taken from NIST Database,[57] while those of Au_{17}, W_2, and Mo_2 are computed at the TPSS/cc-pVDZ-PP + ZPE level.

difficult to detach electron than the M^- and M dopant, respectively. Therefore, the BE values of $M_2@Au_{17}^{0/\pm1}$ are calculated by the following eqs 10−12:

$$BE(M_2@Au_{17}) = [17E(Au) + 2E(M) - E(M_2@Au_{17})]/19 \quad (10)$$

$$BE(M_2@Au_{17}^-) = [16E(Au) + E(Au^-) + 2E(M) - E(M_2@Au_{17}^-)]/19 \quad (11)$$

$$BE(M_2@Au_{17}^+) = [17E(Au) + E(M^+) + E(M) - E(M_2@Au_{17}^+)]/19 \quad (12)$$

Moreover, we find that the pure Au_{17} cluster also has lower IE and higher EA values than the dimer M_2, indicating that it is more difficult for the latter to attach or detach an electron than for the former. Therefore, the DE values of $M_2@Au_{17}^{0/\pm1}$ species are computed as follows (eqs 13−15):

$$DE(M_2@Au_{17}) = E(Au_{17}) + E(M_2) - E(M_2@Au_{17}) \quad (13)$$

$$DE(M_2@Au_{17}^-) = E(Au_{17}^-) + E(M_2) - E(M_2@Au_{17}^-) \quad (14)$$

$$DE(M_2@Au_{17}^+) = E(Au_{17}^+) + E(M_2) - E(M_2@Au_{17}^+) \quad (15)$$

The computed BE and DE values of $M_2@Au_{17}^{0/\pm1}$ are presented in Table 3, which also comprises, for the purpose of comparison, those of the closed size $Au_{19}^{0/\pm1}$ and the well-known magic cluster Au_{20}.[58] Geometries of pure gold clusters

Table 3. Binding Energy per Atom (BE), Dissociation Energy (DE), Vertical Electron Affinity (vEA), Vertical Ionization Energy (vIE), and HOMO−LUMO Gap (HLG) of Clusters Considered[a]

species	BE	DE	vEA	vIE	HLG
	(kcal/mol)		(eV)		
$Mo_2@Au_{17}^-$	62.1	182.5	−0.69	3.02	3.71
$Mo_2@Au_{17}$	60.8	199.7	2.94	6.20	3.26
$Mo_2@Au_{17}^+$	62.2	209.2	6.11	9.46	3.36
$W_2@Au_{17}^-$	65.8	237.7	−0.57	3.03	3.60
$W_2@Au_{17}$	64.5	254.9	2.93	6.14	3.20
$W_2@Au_{17}^+$	67.0	265.2	6.08	9.42	3.34
Au_{19}^-	55.5	77.9	−0.25	3.53	3.78
Au_{19}	53.6	83.1	3.47	6.50	3.04
Au_{19}^+	56.6	76.7	5.86	10.22	4.36
Au_{20}	54.7	87.8	2.51	7.08	4.57

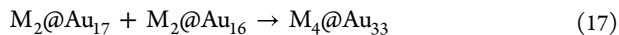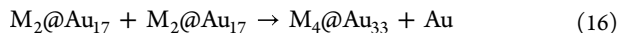[a]Data are collected at the TPSS/cc-pVDZ-PP + ZPE level (kcal/mol).

are collected from recent reports,[55,59,60] and then reoptimized using the TPSS functional with the cc-pVDZ-PP basis set.

As shown in Table 3, the doped $M_2@Au_{17}^{0/\pm1}$ clusters generally have much higher BE and DE values than the pure Au_n systems. The predicted BEs are around 61 and 65 kcal/mol for $Mo_2@Au_{17}$ and $W_2@Au_{17}$, respectively, that are considerably greater than the corresponding values of 54 for Au_{19} and 55 kcal/mol for Au_{20}. In addition, the W_2 dimer is found to induce a stronger influence than the Mo_2. The BE values in the range of 64−67 kcal/mol for $W_2@Au_{17}^{0/\pm1}$ are quite larger than those of $Mo_2@Au_{17}^{0/\pm1}$, being varying from 61 to 62 kcal/mol (Table 3). Likewise, the DE values are predicted to be in the range of 182−209 kcal/mol for $Mo_2@Au_{17}^{0/\pm1}$, as compared to the values of 77−88 kcal/mol for pure gold clusters. The BE between W_2 and $Au_{17}^{0/\pm1}$ of 238−265 kcal/mol also indicates a highly effective guest−host interaction. Previously, the BE between Nb_2 and Au_6 in the highly stable supermolecule $Nb_2@Au_6$ was predicted to be ~200 kcal/mol.[37] The higher stability of $M_2@Au_{17}^q$ as compared to their pure gold counterparts can be understood as a consequence of the fact that an amount of electron has effectively been transferred from the shell to the core. Computed results on the NBO charge distribution of $M_2@Au_{17}^q$, which are summarized in Table S3 of Supporting Information, reveal that the gold atoms are losing electrons while the dopants are acting as electron acceptors. For example, both Mo and W atoms in the neutral **M·1** bear a negative charge of −3.5 and −3.4 electrons, respectively.

Table 3 also includes the HOMO−LUMO energy gap (HLG), a parameter often used to evaluate the kinetic stability and electronic transitions of chemical systems. It is clearly seen that the doped $M_2@Au_{17}^{0/\pm1}$ clusters overall have smaller HLGs than their pure gold counterparts. The HLG values are computed to be 3.7 eV (86 kcal/mol) for $Mo_2@Au_{17}^-$ and 3.6 eV (83 kcal/mol) for $W_2@Au_{17}^-$, which are markedly lower than a corresponding value of 4.6 eV (106 kcal/mol) predicted for the magic tetrahedron Au_{20}.

3.3. Gold-Based Nanowires from $M_2@Au_{17}$.

The search for new nanomaterials with tailor-made electronic and optical properties for relevant applications has become a fundamental challenge for many scientists in chemistry, physics, and nanoscience over the last decades. One of the most promising approaches to creating novel materials is using size-specific

clusters as building units.[61] In this context, a legitimate question is whether the tubular $M_2@Au_{17}$ clusters can be used as a starting unit for the synthesis of gold nanowires. To tackle this query, we now examine the possibility of forming the dimers $M_4@Au_{33}$ based on the following reactions 16 and 17:

$$M_2@Au_{17} + M_2@Au_{17} \rightarrow M_4@Au_{33} + Au \quad (16)$$

$$M_2@Au_{17} + M_2@Au_{16} \rightarrow M_4@Au_{33} \quad (17)$$

The structures of the $M_4@Au_{33}$ dimers are displayed in Figure 2. They are generated by placing one $M_2@Au_{16}$ block
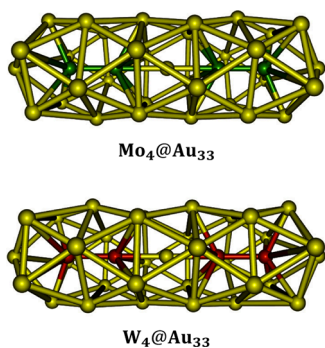

Figure 2. Optimized structures of dimers $M_4@Au_{33}$ (TPSS/cc-pVDZ-PP).

on top of the other connected together by an Au atom playing as a linker. Full vibrational calculations are performed, and both optimized structures are confirmed as real minima with all positive vibrational frequencies.

As shown in Figure 2, each dimer $M_4@Au_{33}$ is formed by assembling two $M_2@Au_{16}$ units along the main axis of the pentagonal antiprism. The building blocks are connected to each other by five-membered Au rings and an Au atom. The shared Au–Au (d_{Au-Au}) bond lengths in $M_4@Au_{33}$ are around 2.95 and 2.98 Å for M = Mo and W, respectively, which are somewhat longer than the d_{M-Au} distances of 2.66 Å between the assembled units. In $Mo_4@Au_{33}$, the d_{Mo-Mo} distance is 2.37 Å, as compared to 2.50 Å in $Mo_2@Au_{17}$. Similarly, the d_{W-W} length of 2.49 Å in $W_4@Au_{33}$ is also quite shorter than a corresponding value of 2.61 Å in $W_2@Au_{17}$.

The thermodynamic stability of $M_4@Au_{33}$ nanowires are analyzed via the BE, the DE, and assembling energies (AE), which are defined by eqs 18−21:

$$BE(M_4@Au_{33}) = [33E(Au) + 4E(M) - E(M_4@Au_{33})] / 37 \quad (18)$$

$$DE(M_4@Au_{33}) = [E(Au_{17}) + E(Au_{16}) + 2E(M_2) - E(M_4@Au_{33})]/2 \quad (19)$$

$$AE_1 = E(M_4@Au_{33}) + E(Au) - 2E(M_2@Au_{17}) \quad (20)$$

$$AE_2 = E(M_4@Au_{33}) - \{E(M_2@Au_{17}) + E(M_2@Au_{16})\} \quad (21)$$

Computed results in Table 4 point out that the BEs of $M_4@Au_{33}$ are ~4 kcal/mol larger than those of $M_2@Au_{17}$. Indeed, these values of $M_4@Au_{33}$ are predicted to be 63 and 67 kcal/mol for M = Mo and W, respectively, as compared to 61 kcal/mol for $Mo_2@Au_{17}$ and 65 kcal/mol for $W_2@Au_{15}$.

For detachment energies, a similar tendency is also observed, but the difference is much more significant (Table 4). Moreover, calculations on the AE with respect to different channels indicate that forming the dimers $M_4@Au_{33}$ from $M_2@Au_{17}$ and $M_2@Au_{16}$ is more energetically favorable than that from two $M_2@Au_{17}$ units. The AE releasing computed by eq 21 are larger than those computed by (20) up to 60 kcal/mol.

3.4. Electronic Structures and Absorption Spectra. The electronic structures and stability patterns of metal clusters have typically been analyzed by the electron shell model. In terms of the phenomenological shell model (PSM),[62] the clusters having a number of valence electrons corresponding to the electronic shells of 1S, 1P, 1D, 2S, 1F, 2P, 1G, and so on tend to exist as a spherical shape and should be particularly stable. For systems not having enough valence electrons to fulfill such electronic shells, either an oblate or a prolate structure is likely to be more preferred, and the energy ordering of the shell orbitals should be tuned. In particular, frontier orbitals that are degenerate in energy should split into various levels to remove the degeneracy and lower the total energy.

Let us analyze the electron shell of the anions $Au_{17}M_2^-$ which has 30 valence electrons, including six electrons from each dopant and one electron from each Au atom. This shell could be formed with an unbalanced electron configuration, i.e., $[1S^2 1P^6 1D^{10} 2S^2 1F^{10}]$, if their equilibrium structures were spherical. As a result of the Jahn–Teller effect, spindle-like structures having D_{5h} symmetry are reached to lower the energy of frontier orbitals.

In the D_{5h}-symmetric crystal-field, degenerate orbitals on the P and D shells split into two and three different subshells, respectively. On the contrary, the 1F orbitals go from a 7-fold degenerate shell in a spherical cluster to four different levels, namely $\{1F_{y(3x^2-y^2)}, 1F_{x(x^2-3y^2)}\}$ (e_2'), $\{1F_{xyz}, 1F_{z(x^2-y^2)}\}$ (e_2''), $\{1F_{xz^2}, 1F_{yz^2}\}$ (e_1'), and $1F_{z^3}$ (a_2'') orbitals. The electron shell of the $M_2@Au_{17}$ species with 30 itinerant electrons can be described as follows:

$$1S^2 1P^6 1D^{10} 2S^2 \{1F_{xz^2}^2 1F_{yz^2}^2\} 1F_{z^3}^2 \{1F_{xyz}^2 1F_{z(x^2-y^2)}^2\}$$

$$\{1F_{y(3x^2-y^2)}, 1F_{x(x^2-3y^2)}\}$$

The $\{1F_{y(3x^2-y^2)}, 1F_{x(x^2-3y^2)}\}$ subshell (Figure 3) now becomes unoccupied and is lying higher in energy than $\{1F_{xz^2}, 1F_{yz^2}\}$, $1F_{z^3}$, and $\{1F_{xyz}, 1F_{z(x^2-y^2)}\}$. Both HOMO and LUMO of the D_{5h} spindle-like anions $M_2@Au_{17}^-$ are degenerate. Therefore, attachment or detachment of an electron is expected to accompany a lowering of its symmetry due to a Jahn–Teller distortion. Indeed, the removal of one electron from these structures should result in a unbalanced configuration with three electrons on the doubly degenerate e_2'' orbitals, i.e., $\{1F_{xyz},$

Table 4. BE, DE, and AE Values (kcal/mol) for $M_4@Au_{33}$ Systems (TPSS/cc-pVDZ-PP + ZPE)

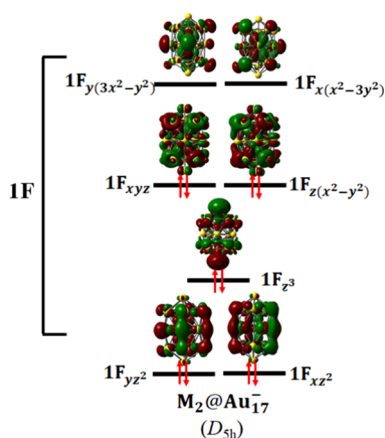| dimer	BE	DE	AE$_1$	AE$_2$	monomer	BE	DE
$Mo_4@Au_{33}$	63.2	245.5	−29.0	−92.9	$Mo_2@Au_{17}$	60.8	199.7
$W_4@Au_{33}$	66.8	296.1	−19.7	−86.5	$W_2@Au_{17}$	64.5	254.9

Figure 3. Splitting of 1F shell orbitals in the D_{5h} cylindrical anions $M_2@Au_{17}^-$.

$1F_{z(x^2-y^2)}$}. Such an electronic degenerate state is not stable, and each cluster tends to undergo a structural relaxation to lower its total energy. The neutral and cationic states are thus more stable in a distorted pentagonal antiprism with C_s and C_{2v} point groups, respectively.

For more insights into interactions between the Au_{17} cage and the dimer, we plot in Figure 4 the partial density of states (PDOS) for the anions $M_2@Au_{17}^-$. The HOMO band of $W_2@Au_{17}^-$ consists of both Au_{17} shell and W_2 core, while the LUMO mostly gives rise from the shell (cf. Figure 4). On the contrary, both the shell and the core contribute almost equally to the HOMO and LUMO bands of $Mo_2@Au_{17}^-$. The calculated PDOS in addition shows a strong hybridization of M-d orbitals with s, p, and d orbitals of Au atoms (Figure 4).

Besides, the unique optical properties of gold clusters and nanoparticles have received great attention in recent years for both basic interest and practical applications. Investigations on small, unsupported clusters as model systems under controlled conditions and without interactions with an outside environment could provide fundamental knowledge that enhances the understanding of more complex systems. Many theoretical and experimental efforts have been devoted to the optical properties of the small gold clusters. At the nanoscale size, classical or semiclassical approaches based on Maxwell's equations for electromagnetic waves coupling with spherical metallic particles can be used to predict the surface plasmon resonance, i.e., a strong optical response giving rise from collective oscillations of valence electrons.[63] However, in order to clarify the molecule-like absorption behaviors of small metal clusters, a full quantum chemical treatment for all valence electrons instead of classical models, is required.[64] It is quite challenging but necessary to probe the optical response of gold clusters due to the strong relativistic effect and active participation of 5d-electrons in gold atoms. Another noteworthy finding is that the inclusion of impurity atoms is inherently accompanied by pronounced impacts on their optical properties, such as decreasing the excitation energy and increasing the dipole moment and oscillator strength.[40]

Using the time-dependent density functional theory (TD-DFT), the optical absorption spectra of $Au_{19}^{0/\pm1}$ and $M_2@Au_{17}^{0/\pm1}$ systems (M = Mo, W) are simulated and presented in Figures 5 and 6. The TD-DFT calculations are carried out on the lowest-lying DFT optimized geometries. Generally, their absorption spectra are dominated by transitions in the visible region. While the absorption spectra of Au_{19}^- and Au_{19}^+ species
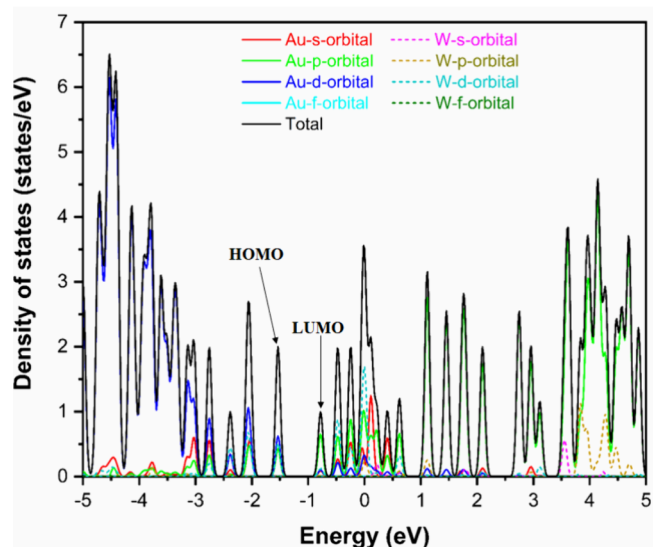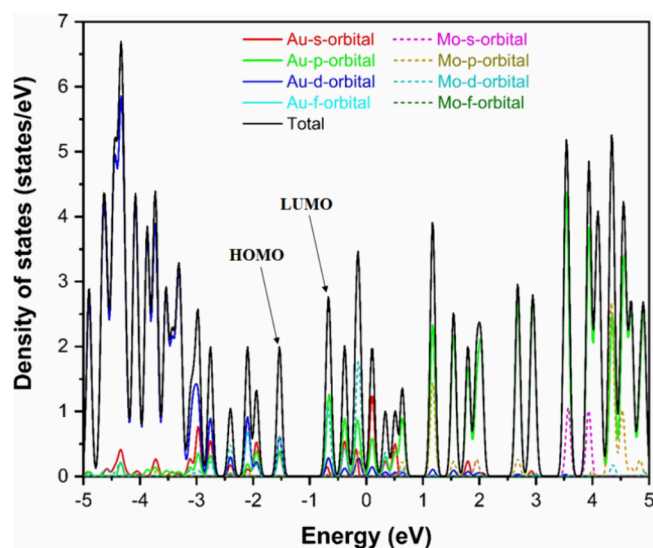

Figure 4. Partial density of states (PDOS) of $Mo_2@Au_{17}^-$ (upper panel) and $W_2@Au_{17}^-$ (lower panel) (TPSS/cc-pVDZ-PP).
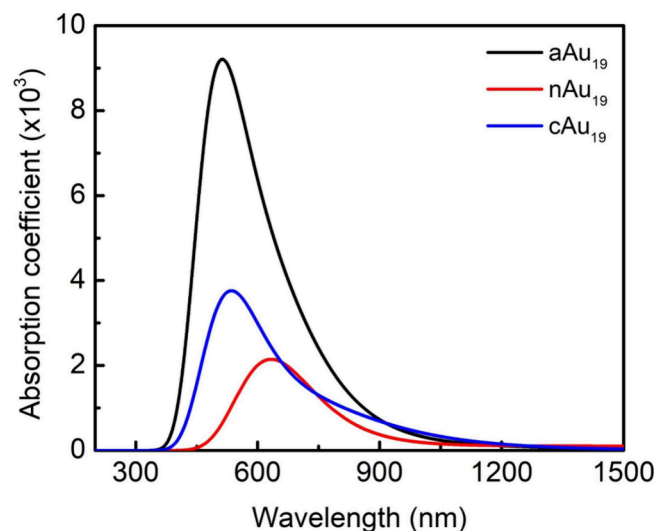

Figure 5. Absorption spectra of the $Au_{19}^{0/\pm1}$ obtained by TD-DFT computations at the TPSS/cc-pVDZ-PP level.
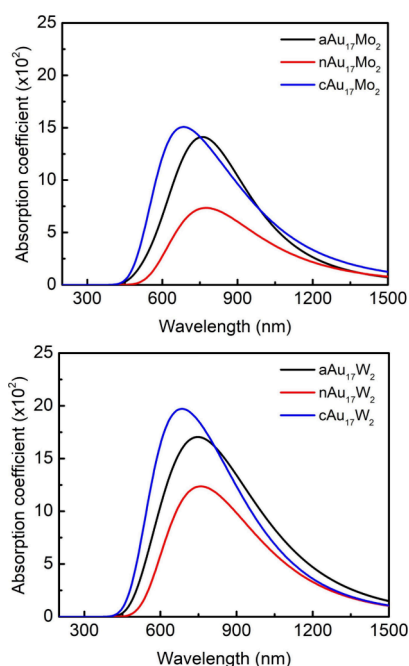
Figure 6. Absorption spectra for $Mo_2@Au_{17}^{0/\pm1}$ (above) and $W_2@Au_{17}^{0/\pm1}$ (below) obtained by TD-DFT computations at the TPSS/cc-pVDZ-PP level.

Au_{19} comprises several electronic transitions giving rise to a broad band in the lower-energy region (Figure 5).

As indicated above, the introduction of Mo and W impurities significantly alters the structures of pure gold clusters. Due to the presence of either Mo_2 or W_2, the cylinder-like shapes with the dopants encapsulated inside turn out to be mostly preferred. Such structural changes should lead to a charge transfer between the host Au_n framework and the dimers M_2 placed inside. As a result, substitution of Mo and W for Au atoms has a huge effect on the optical responses. Indeed, our TD-DFT results show that the major transitions of $M_2@Au_{17}^{0/\pm1}$ systems are remarkably shifted to the longer wavelength region (Figure 6). For doped systems, the optical absorption bands centered below 600 nm are strongly suppressed, and the intensity is also greatly decreased. The major absorption peaks for $M_2@Au_{17}^{0/\pm1}$ are now observed in the range between 650 and 800 nm, while those of $Au_{19}^{0/\pm1}$ are typically located below 600 nm.

3.5. Optical Nonlinearity. Due to their structural diversity, gold-based clusters typically exhibit unique optical properties that are challenging but worth probing. Thus, we carry out further calculations on the dipole moment, polarizability, and first and second hyperpolarizability for the clusters in their ground state structures to examine their linear and NLO characteristics. In this section, the LC-BLYP functional is employed in conjunction with the cc-pVDZ-PP basis set. The rationale for the selection of such an approach is given below.

Typically, benchmark studies have often used para-nitroaniline (p-NA) to test the accuracy and suitability of the methods employed. Table S4 (Supporting Information) lists the calculated gas-phase dipole moment and frequency-dependent polarizability tensors of p-NA, along with the available experimental data for comparison. For the static dipole

are identified by intense peaks near 500 and 540 nm, respectively (Figure 6), that of Au_{19} is characterized by a much lower intensity band centered at 630 nm (Figure 5). As compared to the closed-shell systems $Au_{19}^{\mp}$, neutral Au_{19} with an open-shell electronic structure tends to exhibit a more complicated absorption feature. The absorption spectrum of

Table 5. Gas-Phase Dipole Moment (μ), Isotropic (α_{iso}), and Anisotropic (α_{aniso}) Polarizabilities, and First-Order (β) and Second-Order (γ) Hyperpolarizabilities in Atomic Unit (a.u.) of Au_{19}^q, $M_2@Au_{17}^q$ Clusters, and the p-NA Molecule[a]

		$Mo_2 @ Au_{17}^q$			$W_2 @ Au_{17}^q$			Au_{19}^q			
q		−1	0	+1	−1	0	+1	−1	0	+1	p-NA
μ		0.0	0.31	0.47	0.0	0.27	0.51	0.39	0.60	0.35	2.77
α											
α_{iso}	(0)	609.9	583.3	555.5	610.5	547.6	555.1	757.4	757.3	608.2	99.2
	($-\omega$)	636.7	608.8	585.1	635.1	586.3	581.0	804.4	747.2	638.6	101.0
α_{aniso}	(0)	193.3	181.8	182.8	192.8	121.9	188.0	66.0	82.0	100.7	78.2
	($-\omega$)	200.7	230.5	257.8	199.0	174.2	251.5	67.7	70.0	118.3	81.2
β											
β_{tot}	(0)	0.05	2187.6	1667.6	0.04	2577.1	1276.2	2983.8	8910.5	422.7	1177.9
	($-\omega$)	0.22	1100.1	1430.0	0.04	233.7	1479.5	3928.8	36942.2	526.4	1333.5
	(-2ω)	17.5	36.6	387.7	2.22	209.3	1574.1	28047.2	23979.4	1634.2	1755.1
$\beta_\parallel$	(0)	0.0	−1312.6	−1000.6	0.0	−1546.2	−765.7	−1790.3	−2930.2	−253.6	702.6
	($-\omega$)	0.0	−660.1	−858.0	0.0	−140.2	−887.7	−2357.3	−22147.1	−315.9	795.4
	(-2ω)	0.0	22.0	−232.6	0.0	−125.5	−944.4	−16828.3	−12357.8	−980.5	1046.9
$\gamma/10^4$											
γ_{tot}	(0)	24.0	16.2	8.98	24.9	16.7	8.37	37.7	22.8	9.04	2.03
	($-\omega$)	25.9	11.0	7.78	31.5	42.6	7.76	49.4	31.8	10.1	2.33
	(-2ω)	21.0	81.5	13.9	30.1	23.3	27.7	42.0	32.9	15.2	3.20
$\gamma_\parallel$	(0)	39.6	25.5	14.3	41.7	28.1	14.2	61.3	39.2	15.6	2.55
	($-\omega$)	41.6	18.1	6.51	53.3	60.3	8.19	85.3	54.5	17.3	2.88
	(-2ω)	32.0	118.4	19.0	47.6	40.2	46.5	58.1	51.7	25.9	3.80

[a]Dynamic (hyper) polarizabilities are computed at the fundamental wavelength of λ = 1064 nm, using the LC-BLYP functional and cc-pVDZ-PP basis set.

moment (μ), we find that all functionals considered are likely to overestimate the experimental value. As compared to the experimental value of $\mu = 2.70$ a.u., either wB97XD or LC-BLYP appears to provide a more reliable result than other approaches. Moreover, based on the LC-BLYP/aDZ calculation, a $\beta_\parallel(-2\omega, \omega, \omega) = 1046.9$ (a.u.) at 1064 nm is obtained for p-NA, which is also in good agreement with the corresponding value of 1072 ± 44 a.u. measured in the gas phase.[65] On the contrary, other functionals tend to greatly overestimate the experimental result. Overall, the LC-BLYP long-range corrected functional is found to properly reproduce the experimental μ and β values for p-NA, and it is thus selected for evaluation of NLO properties of the clusters considered.

The static and dynamic polarizabilities for $M_2@Au_7^q$ clusters computed with the LC-BLYP functional are listed in Table 5. Accordingly, the anions $M_2@Au_{17}^-$ have larger values of α_{iso} than their neutral and cationic counterparts. The dynamic isotropic polarizabilities of $M_2@Au_7^q$ are predicted to be in the range of 547−611 a.u., which are quite lower than those predicted for the pure gold systems. Thus, the replacement of Au by Mo and W atoms decreases the polarizability of Au_{19}^q species. Furthermore, the dynamic polarizability of both $M_2@Au_7^q$ and Au_{19}^q typically has values higher than the static one, except for the Au_{19} cluster. Moreover, as compared to an external reference, these clusters have particularly large values of α_{iso}, being from 5.75 to 7.96 times greater than p-NA. Except for the anion Au_{19}^-, all clusters considered also exhibit slightly higher values of α_{aniso} than p-NA. The largest and smallest dynamic anisotropic polarizabilities of 257.8 and 67.8 a.u. are obtained for $Mo_2@Au_{17}^+$ and Au_{19}^- clusters, respectively, as compared to a corresponding value of 81.2 a.u. for the p-NA molecule.

As the hyperpolarizabilities are proportional to the electric dipole moment, the systems without dipole moment like, $Mo_2@Au_{17}^-$ and $W_2@Au_{17}^-$, have almost zero values of β components, implying that they do not have a pronounced NLO activity. However, their neutral and cationic counterparts show significant nonlinearity. In particular, $Mo_2@Au_{17}$ and $W_2@Au_{17}$ have a value of $\beta_{tot}(0)$ around 2188 and 2577 a.u., respectively, which are much smaller than the corresponding value of 8911 au obtained for Au_{19}, but almost two times larger than that of the highly π-delocalized p-NA (1178 a.u.).

Overall, the β values for $M_2@Au_7^q$ undergo a significant reduction, compared to that of the pure gold counterparts. Such a phenomenon was also observed for Au_nM systems ($n = 17, 19$; $M = Cu, Ag$).[66] We in addition note that, while the dynamic values for Au_{19}^q clusters follow the expected order of $\beta(0) < \beta(-\omega) < \beta(-2\omega)$, the doped clusters only show a similar trend for $W_2@Au_{17}^+$. Another noticeable result is the negative values of the β component in the direction of μ, i.e., the $\beta_\parallel$ value, for both pure and doped gold clusters. This reflects a negative change of dipole moments following excitation from the ground to the excited states.[67]

The computed results for static and dynamic second-order hyperpolarizabilities of $M_2@Au_7^q$ clusters are also collected in Table 5. For $Mo_2@Au_7^q$, $W_2@Au_7^q$, and Au_{19}^q clusters, the static $\gamma_{tot}(0)$ values are in the range of 9.0−24.0, 8.4−24.9, and 9.0−37.7 ($\times 10^4$ a.u.), respectively, that are much larger than the corresponding value of 2.0×10^4 a.u. obtained for p-NA. Noticeably, the anions $M_2@Au_{17}^-$ are found to have particularly large values of static second-order hyperpolarizabilities, while the β components are almost zero (Table 5). Thus, it is likely

that they exhibit an excellent NLO activity related to the hyperfine structure,[67] although the NLO response is rather weak in the second-order fine structure. Computed results listed in Table 5 in addition reveal that the second dynamic hyperpolarizability of both pure and doped gold clusters is typically larger than the static one, but not always following a correct order, $\gamma(0) < \gamma(-\omega) < \gamma(-2\omega)$, as in the p-NA molecule. Moreover, the cluster in anionic states is predicted to have larger γ values, both static and dynamic, than the corresponding cation, even though the former is more symmetric and has a dipole moment lower than that of the latter.

4. CONCLUDING REMARKS

In the present theoretical study, we presented the structure, stability, and electronic and optical nonlinearity properties of the cylindrical $M_2@Au_7^q$ clusters that were thoroughly investigated using quantum chemical computations with the DFT and TD-DFT approaches. In contrast to the pure Au_n clusters up to $n = 20$, a tube-like form with a dopant dimer M_2 encapsulated inside an Au_{17} framework along the symmetry axis was found for the first time as the dominant structure of the doped $M_2@Au_7^q$ species. Energetic calculations for several parameters, such as the BE per atom and DE, show that the presence of Mo_2 and W_2 units significantly enhances the stability of the gold clusters. Their effects on the electronic structures and optical responses are also remarkable.

The absorption spectra of $M_2@Au_7^q$ species are characterized by major electronic transitions in the range of 650−800 nm rather than below 600 nm as in the pure clusters $Au_{19}^{0/\pm1}$. These binary systems emerge as ideal building blocks for the formation of gold-assembled nanowires, which are connected together by the five-membered Au rings and an Au atom.

We in addition examine the NLO properties of $Au_{17}M_2^q$ clusters in comparison with those of $Au_{19}^{0/\pm1}$ clusters and p-nitropaniline (p-NA) molecules based on the static and dynamic (hyper) polarizability tensors. The hyperpolarizabilities of clusters were found to undergo a significant reduction upon replacement of Au atoms by Mo_2 and W_2 units but remain much larger than those of p-NA. The neutrals $M_2@Au_{17}$ are expected to exert excellent optical responses as they exhibit exceptionally high values for both the first- and second-order NLO coefficients. Present results reveal that these pure and doped gold clusters are good materials to be considered for different optoelectronic features.

■ ASSOCIATED CONTENT

Data Availability Statement

Quantum chemical computations were carried out using the Gaussian 16 program. The main isomers optimized are given in the Supporting Information.

Ⓢ Supporting Information

The Supporting Information is available free of charge at https://pubs.acs.org/doi/10.1021/acsomega.4c02724.

> Ground state structures of Au_{19}^q clusters located at the TPSS/cc-pVDZ-PP level; optimized geometries and Cartesian coordinates of $M_2@Au_7^q$ isomers; Cartesian coordinates of the dimers $M_4@Au_{33}$; natural charges distributed on Mo and W atoms in $M_2 @ Au_{17}^{0/\pm1}$ clusters computed at the TPSS/cc-pVTZ-PP level; and gas-phase dipole moment and first hyperpolarizability tensors in atomic unit of p-NA (PDF)

AUTHOR INFORMATION

Corresponding Author

Minh Tho Nguyen − *Laboratory for Chemical Computation and Modeling, Institute for Computational Science and Artificial Intelligence and Faculty of Applied Technology, School of Technology, Van Lang University, Ho Chi Minh 70000, Vietnam;* ● orcid.org/0000-0002-3803-0569; Email: minhtho.nguyen@vlu.edu.vn

Authors

Pham Vu Nhat − *Molecule and Materials Modeling Laboratory, Department of Chemistry, Can Tho University, Can Tho 90000, Vietnam;* ● orcid.org/0000-0002-1485-6569

Nguyen Thi Bao Trang − *School of Education, Can Tho University, Can Tho 90000, Vietnam*

Minh Triet Dang − *School of Education, Can Tho University, Can Tho 90000, Vietnam;* ● orcid.org/0000-0003-1769-4873

Nguyen Thanh Si − *Institute of Environmental Science and Technology, Tra Vinh University, Tra Vinh 94000, Vietnam*

Tran Thi Ngoc Thao − *Department of Physics, Can Tho University, Can Tho 90000, Vietnam*

Pham Thi Bich Thao − *Department of Physics, Can Tho University, Can Tho 90000, Vietnam*

Complete contact information is available at:
https://pubs.acs.org/10.1021/acsomega.4c02724

Notes

The authors declare no competing financial interest.

ACKNOWLEDGMENTS

REFERENCES

(1) Teles, J. H.; Brode, S.; Chabanas, M. Cationic gold (I) complexes: highly efficient catalysts for the addition of alcohols to alkynes. *Angew. Chem., Int. Ed. Engl.* **1998**, *37*, 1415−1418.

(2) Veenboer, R. M.; Dupuy, S.; Nolan, S. P. Stereoselective gold (I)-catalyzed intermolecular hydroalkoxlation of alkynes. *ACS catalysis* **2015**, *5*, 1330−1334.

(3) Rudolph, M.; Hashmi, A. S. K. Heterocycles from gold catalysis. *Chem. Commun.* **2011**, *47*, 6536−6544.

(4) Saha, K.; Agasti, S. S.; Kim, C.; Li, X.; Rotello, V. M. Gold nanoparticles in chemical and biological sensing. *Chem. Rev.* **2012**, *112*, 2739−2779.

(5) Austin, L. A.; Mackey, M. A.; Dreaden, E. C.; El-Sayed, M. A. The optical, photothermal, and facile surface chemical properties of gold and silver nanoparticles in biodiagnostics, therapy, and drug delivery. *Arch. Toxicol.* **2014**, *88*, 1391−1417.

(6) Wallace, W. T.; Whetten, R. L. Carbon Monoxide Adsorption on Selected Gold Clusters: Highly Size-Dependent Activity and Saturation Compositions. *J. Phys. Chem. B* **2000**, *104*, 10964−10968.

(7) Sanchez, A.; Abbet, S.; Heiz, U.; Schneider, W. D.; Häkkinen, H.; Barnett, R. N.; Landman, U. When Gold Is Not Noble: Nanoscale Gold Catalysts. *J. Phys. Chem. A* **1999**, *103*, 9573−9578.

(8) Hainfeld, J.; Slatkin, D.; Focella, T.; Smilowitz, H. Gold nanoparticles: a new X-ray contrast agent. *Br. J. Radiol.* **2006**, *79*, 248.

(9) Huyen, D. T.; Bui, T. Q.; Si, N. T.; Nhat, P. V.; Quy, P. T.; Nhung, N. T. A. Theoretical study of the binding mechanism between anticancerous drug mercaptopurine and gold nanoparticles using a cluster model. *J. Mol. Model.* **2023**, *29*, 307.

(10) Kha, T. N.; Si, N. T.; Tran, V. M.; Vo, K. Q.; Nguyen, M. T.; Nhat, P. V. Binding Mechanism and Surface-Enhanced Raman Scattering of the Antimicrobial Sulfathiazole on Gold Nanoparticles. *ACS Omega* **2023**, *8*, 43442−43453.

(11) Zheng, J.; Dickson, R. M. Individual water-soluble dendrimer-encapsulated silver nanodot fluorescence. *J. Am. Chem. Soc.* **2002**, *124*, 13982−13982.

(12) Vosch, T.; Antoku, Y.; Hsiang, J. C.; Richards, C. I.; Gonzalez, J. I.; Dickson, R. M. Strongly emissive individual DNA-encapsulated Ag nanoclusters as single-molecule fluorophores. *Proc. Natl. Acad. Sci. U. S. A.* **2007**, *104*, 12616−12621.

(13) Fenwick, O.; Coutiño-Gonzalez, E.; Grandjean, D.; Baekelant, W.; Richard, F.; Bonacchi, S.; Vos, D. D.; Lievens, P.; Roeffaers, M.; Hofkens, J.; Samorì, P. Tuning the energetics and tailoring the optical properties of silver clusters confined in zeolites. *Nat. Mater.* **2016**, *15*, 1017−1022.

(14) Collings, B. A.; Athanassenas, K.; Rayner, D. M.; Hackett, P. A. Optical spectroscopy of Ag_7, Ag_9^+, and Ag_9. A test of the photodepletion method. *Chem. Phys. Lett.* **1994**, *227*, 490−495.

(15) Krückeberg, S.; Dietrich, G.; Lützenkirchen, K.; Schweikhard, L.; Walther, C.; Ziegler, J. The dissociation channels of silver clusters Ag_n^+, $3 \le n \le 20$. *Int. J. Mass Spectrom.* **1996**, *155*, 141−148.

(16) Harb, M.; Rabilloud, F.; Simon, D.; Rydlo, A.; Lecoultre, S.; Conus, F.; Rodrigues, V.; Félix, C. Optical absorption of small silver clusters: Ag_n, (n = 4 − 22). *J. Chem. Phys.* **2008**, *129*, 194108.

(17) Shayeghi, A.; Götz, D. A.; Johnston, R. L.; Schäfer, R. Optical absorption spectra and structures of Ag_6^+ and Ag_8^+. *Eur. Phys. J. D* **2015**, *69*, 152.

(18) Xu, X.; Truhlar, D. G. Accuracy of Effective Core Potentials and Basis Sets for Density Functional Calculations, Including Relativistic Effects, As Illustrated by Calculations on Arsenic Compounds. *J. Chem. Theory Comput.* **2011**, *7*, 2766−2779.

(19) Lu, T.; Chen, F. Multiwfn: A multifunctional wavefunction analyzer. *J. Comput. Chem.* **2012**, *33*, 580−592.

(20) Nhat, P. V.; Si, N. T.; Fielicke, A.; Kiselev, V. G.; Nguyen, M. T. A new look at the structure of the neutral Au_{18} cluster: hollow versus filled golden cage. *Phys. Chem. Chem. Phys.* **2023**, *25*, 9036−9042.

(21) Borin, A. C.; Gobbo, J. P.; Roos, B. O. A theoretical study of the binding and electronic spectrum of the Mo_2 molecule. *Chem. Phys.* **2008**, *343*, 210−216.

(22) Nhat, P. V.; Si, N. T.; Kiselev, V. G.; Fielicke, A.; Pham, H. T.; Nguyen, M. T. Unexpected structures of the Au_{17} gold cluster: the stars are shining. *Chem. Commun.* **2022**, *58*, 5785−5788.

(23) Wang, L.-M.; Bai, J.; Lechtken, A.; Huang, W.; Schooss, D.; Kappes, M. M.; Zeng, X. C.; Wang, L.-S. Magnetic doping of the golden cage cluster $M@Au_{16}^-$ (M = Fe, Co, Ni). *Phys. Rev. B* **2009**, *79*, No. 033413.

(24) Wang, H.-Q.; Li, H.-F.; Zheng, L.-X. Doping golden cage clusters $M@Au_{16}^q$ (M = Cr, Mn; q = 0,−1) with adjustable magnetic properties. *J. Magn. Magn. Mater.* **2013**, *344*, 79−84.

(25) Li, H.-F.; Wang, H.-Q. Probing the stability of neutral and anionic transition-metal-doped golden cage nanoclusters: $M@Au_{16}$ (M= Sc, Ti, V). *Phys. Chem. Chem. Phys.* **2014**, *16*, 244−254.

(26) Gao, Y.; Bulusu, S.; Zeng, X. C. Gold-caged metal clusters with large HOMO-LUMO gap and high electron affinity. *J. Am. Chem. Soc.* **2005**, *127*, 15680−15681.

(27) Gao, Y.; Bulusu, S.; Zeng, X. C. A Global Search of Highly Stable Gold-Covered Bimetallic Clusters $M@Au_n$ (n = 8−17): Endohedral Gold Clusters. *ChemPhysChem* **2006**, *7*, 2275−2278.

(28) Pyykkö, P.; Runeberg, N. Icosahedral WAu_{12}: A Predicted Closed-Shell Species, Stabilized by Aurophilic Attraction and Relativity and in Accord with the 18-Electron Rule. *Angew. Chem., Int. Ed.* **2002**, *41*, 2174−2176.

(29) Nhat, P. V.; Tai, T. B.; Nguyen, M. T. Theoretical study of Au_nV-CO, n = 1−14: The dopant vanadium enhances CO adsorption on gold clusters. *J. Chem. Phys.* **2012**, *137*, 164312.

(30) Kaydashev, V. E.; Janssens, E.; Lievens, P. Optical absorption spectra of palladium doped gold cluster cations. *J. Chem. Phys.* **2015**, *142*, No. 034310.

(31) Ferrari, P.; Molina, L. M.; Kaydashev, V. E.; Alonso, J. A.; Lievens, P.; Janssens, E. Controlling the Adsorption of Carbon Monoxide on Platinum Clusters by Dopant-Induced Electronic Structure Modification. *Angew. Chem., Int. Ed.* **2016**, *128*, 11225−11229.

(32) Abdulhussein, H. A.; Ferrari, P.; Vanbuel, J.; Heard, C.; Fielicke, A.; Lievens, P.; Janssens, E.; Johnston, R. L. Altering CO binding on gold cluster cations by Pd-doping. *Nanoscale* **2019**, *11*, 16130−16141.

(33) Li, Y.-F.; Li, Y.; Kuang, X.-Y. Probing the structural and electronic properties of bimetallic Group-III metal-doped gold clusters: Au_nM_2 (M = Na, Mg, Al; n = 1−8). *Eur. Phys. J. D* **2013**, *67*, 132.

(34) Li, Y.; Cao, Y. P.; Li, Y. F.; Shi, S. P.; Kuang, X. Y. DFT study on size-dependent geometries, stabilities, and electronic properties of Au_nM_2 (M = Si, P; n = 1−8) clusters. *Eur. Phys. J. D* **2012**, *66*, 10.

(35) Bhattacharjee, D.; Mishra, B. K.; Deka, R. C. Effect of double aluminium doping on the structure, stability and electronic properties of small gold clusters. *J. Mater. Sci.* **2015**, *50*, 4586−4599.

(36) Jian, T.; Cheung, L. F.; Chen, T.-T.; Lopez, G. V.; Li, W.-L.; Wang, L.-S. Di-niobium gold clusters: Multiply-bonded Nb_2 dimer coordinated equatorially by Au atoms. *Int. J. Mass Spectrom.* **2018**, *434*, 7−16.

(37) Jian, T.; Cheung, L. A.-O.; Czekner, J. A.-O.; Chen, T. T.; Lopez, G. V.; Li, W. L.; Wang, L. A.-O. $Nb_2@Au_6$: a molecular wheel with a short Nb≡Nb triple bond coordinated by an Au_6 ring and reinforced by σ aromaticity. *Chem. Sci.* **2017**, *8*, 7528−7536.

(38) Roundhill, D. M.; Fackler, J. P. *Optoelectronic Properties of Inorganic Compounds*; Springer: US, 2013.

(39) Raza Ayub, A.; Aqil Shehzad, R.; Alarfaji, S. S.; Iqbal, J. Super alkali (OLi_3) doped boron nitride with enhanced nonlinear optical behavior. *J. Nonlinear Opt. Phys. Mater.* **2020**, *29*, 2050004.

(40) Hussain, F.; Hussain, R.; Adnan, M.; Muhammad, S.; Irshad, Z.; Khan, M. U.; Yaqoob, J.; Ayub, K. Insights into the nonlinear optical (NLO) response of pure Au_m (2 ≥ m ≤ 7) and copper-doped $Au_m−xCu_x$ clusters. *RSC Adv.* **2022**, *12*, 25143−25153.

(41) Kosar, N.; Mahmood, T.; Ayub, K.; Tabassum, S.; Arshad, M.; Gilani, M. A. Doping superalkali on $Zn_{12}O_{12}$ nanocage constitutes a superior approach to fabricate stable and high-performance nonlinear optical materials. *Optics & Laser Technology* **2019**, *120*, No. 105753.

(42) Banerjee, A.; Ghanty, T. K.; Chakrabarti, A.; Kamal, C. Nonlinear Optical Properties of $Au_{19}M$ (M = Li, Na, K, Rb, Cs, Cu, Ag) Clusters. *J. Phys. Chem. C* **2012**, *116*, 193−200.

(43) Nhat, P. V.; Si, N. T.; Hang, N. T. N.; Nguyen, M. T. The lowest-energy structure of the gold cluster Au_{10}: planar vs. nonplanar? *Phys. Chem. Chem. Phys.* **2021**, *24*, 42−47.

(44) Tao, J.; Perdew, J. P.; Staroverov, V. N.; Scuseria, G. E. Climbing the density functional ladder: Nonempirical meta−generalized gradient approximation designed for molecules and solids. *Phys. Rev. Lett.* **2003**, *91*, No. 146401.

(45) Peterson, K. A.; Puzzarini, C. Systematically convergent basis sets for transition metals. II. Pseudopotential-based correlation consistent basis sets for the group 11 (Cu, Ag, Au) and 12 (Zn, Cd, Hg) elements. *Theor. Chem. Acc.* **2005**, *114*, 283−296.

(46) Frisch, M. J.; Trucks, G. W.; Schlegel, H. B.; Scuseria, G. E.; Robb, M. A.; Cheeseman, J. R.; Scalmani, G.; Barone, V.; Petersson, G. A.; Nakatsuji, H.; Li, X.; Caricato, M.; Marenich, A. V.; Bloino, J.; Janesko, B. G.; Gomperts, R.; Mennucci, B.; Hratchian, H. P.; Ortiz, J. V.; Izmaylov, A. F.; Sonnenberg, J. L.; Williams; Ding, F.; Lipparini, F.; Egidi, F.; Goings, J.; Peng, B.; Petrone, A.; Henderson, T.; Ranasinghe, D.; Zakrzewski, V. G.; Gao, J.; Rega, N.; Zheng, G.; Liang, W.; Hada, M.; Ehara, M.; Toyota, K.; Fukuda, R.; Hasegawa, J.; Ishida, M.; Nakajima, T.; Honda, Y.; Kitao, O.; Nakai, H.; Vreven, T.; Throssell, K.; Montgomery, Jr., J. A.; Peralta, J. E.; Ogliaro, F.; Bearpark, M. J.; Heyd, J. J.; Brothers, E. N.; Kudin, K. N.; Staroverov, V. N.; Keith, T. A.; Kobayashi, R.; Normand, J.; Raghavachari, K.; Rendell, A. P.; Burant, J. C.; Iyengar, S. S.; Tomasi, J.; Cossi, M.; Millam, J. M.; Klene, M.; Adamo, C.; Cammi, R.; Ochterski, J. W.; Martin, R. L.; Morokuma, K.; Farkas, O.; Foresman, J. B.; Fox, D. J. *Gaussian 16 Rev. C.01*; Wallingford, CT, 2016.

(47) Zhang, G.; Musgrave, C. B. Comparison of DFT Methods for Molecular Orbital Eigenvalue Calculations. *J. Phys. Chem. A* **2007**, *111*, 1554−1561.

(48) Weigend, F.; Ahlrichs, R. Quantum Chemical Treatments of Metal Clusters. *Philosophical transactions. Series A, Mathematical, physical, and engineering sciences* **2010**, *368*, 1245−1263.

(49) Cramer, C. J.; Truhlar, D. G. Density functional theory for transition metals and transition metal chemistry. *Phys. Chem. Chem. Phys.* **2009**, *11*, 10757−10816.

(50) Tsuneda, T.; Song, J.-W.; Suzuki, S.; Hirao, K. On Koopmans' Theorem in Density Functional Theory. *J. Chem. Phys.* **2010**, *133*, 174101.

(51) Munoz-Castro, A. Triple 1D≡1D superatomic bonding. $Au_{22}(dppo)_6$ as a $Π^{4−}$- and $Δ^2$-triply bonded cluster based on Au_{11} assembled units. *Phys. Chem. Chem. Phys.* **2020**, *22*, 1422−1426.

(52) Munoz-Castro, A. Single, double, and triple intercluster bonds: analyses of M2Au36(SR)24 (M = Au, Pd, Pt) as 14-, 12- and 10-ve superatomic molecules. *Chem. Commun. (Camb)* **2019**, *55*, 7307−7310.

(53) Wang, Y.-L.; Hu, H.-S.; Li, W.-L.; Wei, F.; Li, J. Relativistic Effects Break Periodicity in Group 6 Diatomic Molecules. *J. Am. Chem. Soc.* **2016**, *138*, 1126−1129.

(54) Xing, X.; Yoon, B.; Landman, U.; Parks, J. H. Structural evolution of Au nanoclusters: From planar to cage to tubular motifs. *Phys. Rev. B* **2006**, *74*, No. 165423.

(55) Ferrari, P.; Janssens, E. Argon Adsorption on Cationic Gold Clusters Aun+ (n ≤ 20). *Molecules [Online]* **2021**, *26*, 4082.

(56) Nhat, P. V.; Si, N. T.; Leszczynski, J.; Nguyen, M. T. Another look at structure of gold clusters Aun from perspective of phenomenological shell model. *Chem. Phys.* **2017**, *493*, 140−148.

(57) NIST Atomic Spectra Database Ionization Energies Form. https://physics.nist.gov/PhysRefData/ASD/ionEnergy.html.

(58) Pople, J. A.; Head-Gordon, M.; Raghavachari, K. Quadratic configuration interaction. A general technique for determining electron correlation energies. *J. Chem. Phys.* **1987**, *87*, 5968−5975.

(59) Bulusu, S.; Li, X.; Wang, L.-S.; Zeng, X. C. Evidence of hollow golden cages. *Proc. Natl. Acad. Sci. U. S. A.* **2006**, *103*, 8326−8330.

(60) Wang, L.-M.; Bulusu, S.; Zhai, H.-J.; Zeng, X.-C.; Wang, L.-S. Doping golden buckyballs: Cu@Au16−and Cu@Au17−cluster anions. *Angew. Chem., Int. Ed. Engl.* **2007**, *46*, 2915−2918.

(61) Qian, M.; Reber, A. C.; Ugrinov, A.; Chaki, N. K.; Mandal, S.; Saavedra, H. M.; Khanna, S. N.; Sen, A.; Weiss, P. S. Cluster-Assembled Materials: Toward Nanomaterials with Precise Control over Properties. *ACS Nano* **2010**, *4*, 235−240.

(62) Knight, W. D.; Clemenger, K.; de Heer, W. A.; Saunders, W. A.; Chou, M. Y.; Cohen, M. L. Electronic Shell Structure and Abundances of Sodium Clusters. *Phys. Rev. Lett.* **1984**, *52*, 2141−2143.

(63) Idrobo, J. C.; Walkosz, W.; Yip, S. F.; Öğüt, S.; Wang, J.; Jellinek, J. Static polarizabilities and optical absorption spectra of gold clusters (Aun, n = 2−14 and 20) from first principles. *Phys. Rev. B* **2007**, *76*, No. 205422.

(64) Anak, B.; Bencharif, M.; Rabilloud, F. Time-dependent density functional study of UV-visible absorption spectra of small noble metal clusters (Cun, Agn, Aun, n = 2−9, 20). *RSC Adv.* **2014**, *4*, 13001−13011.

(65) Kaatz, P.; Donley, E. A.; Shelton, D. P. A comparison of molecular hyperpolarizabilities from gas and liquid phase measurements. *J. Chem. Phys.* **1998**, *108*, 849−856.

(66) Tang, C.; Zhu, W.; Zhang, K.; He, X.; Zhu, F. The density functional studies of the doped gold cages Au17M (M = Cu, Ag, Li, Na, K). *Comput. Theor. Chem.* **2014**, *1049*, 62−66.

(67) Di Bella, S.; Fragalà, I.; Guerri, A.; Dapporto, P.; Nakatani, K. Synthesis, crystal structure, and second-order nonlinear optical properties of [N,N′-bis(1H-pyrrol-2-ylmethylene)-1,2-benzenediaminato]nickel(II) Schiff base complexes. *Inorg. Chim. Acta* **2004**, *357*, 1161−1167.